Archaeometric analysis of Roman bronze coins from the *Magna Mater* temple using solid-state voltammetry and electrochemical impedance spectroscopy

Francesca Di Turo[a], Noemí Montoya[b], Joan Piquero-Cilla[b], Caterina De Vito[a], Fulvio Coletti[c], Gabriele Favero[d], Antonio Doménech-Carbó*[b]

[a] Department of Earth Sciences, Sapienza University of Rome, P.le Aldo Moro 5, Rome, Italy.
[b] Departament de Química Analítica. Universitat de València. Dr. Moliner, 50, 46100 Burjassot (València) Spain.
[c] Soprintendenza Speciale per il Colosseo, il Museo Nazionale Romano e l'Area Archeologica di Roma, P.zza dei Cinquecento 67, Rome, Italy.
[d] Department of Chemistry and Drug Technologies, Sapienza University of Rome, P.le Aldo Moro 5, Rome, Italy.

* Corresponding author: e-mail: antonio.domenech@uv.es.

Abstract

The application of the voltammetry of microparticles (VMP) and electrochemical impedance spectroscopy (EIS) techniques to a set of 15 Roman bronze coins and one *Tessera* from the temple of *Magna Mater* (Rome, Italy) found in a context dated back between the second half and the end of the 4th century A.D. but having a complicated stratigraphy is described. Characteristic voltammetric patterns for cuprite and tenorite for sub-microsamples of the corrosion layers of the coins attached to graphite electrodes in contact with 0.10 M $HClO_4$ aqueous solution yielded a grouping of the coins into three main groups. This grouping was confirmed and refined using EIS experiments of the coins immersed in air-saturated mineral water using the reduction of dissolved oxygen as a redox probe. The analysis carried out on the surface of the samples corroborates the complex stratigraphy of the archaeological site and, more important, the reuse of the coins during the later periods due to the economic issues related to the fall of the Roman Empire.

Keywords: Roman coins; voltammetry of microparticles; electrochemical impedance spectroscopy; bronze; corrosion.

Introduction

The analysis of archaeological artefacts needs non-invasive and non-destructive techniques due to the significance of this kind of samples and in literature is possible to find an extensive application of different techniques to the study of archaeological materials [1-9]. In particular, metals and alloys had a key role in human history, characterizing historical periods and influencing the technological background and the social life of ancient populations. The knowledge of this kind of materials and their corrosion products can provide information on the technological level reached from ancient populations as well as on post-manufacturing processes, helping the archaeologists to find an answer to dating, provenance and authentication's questions [10,11]. Furthermore, the knowledge about the composition of the metal materials and its corrosion products helps to choose the appropriate treatment of restoration and conservation [12-14].

Bronze is an alloy extensively used in the past and its composition is mainly made of copper and tin, which can often contain other elements such as zinc and lead at different concentration. The conservation of bronze can be affected by several factors, such as temperature, humidity, acid rain, atmospheric particulate matter, sulfur oxides, nitrogen oxides and marine aerosol [4,5,12], and at least, burial condition that determine the formation of the patina. The primary patina is a first layer of metal oxides formed since the usage period of the object, accompanied by a secondary patina, resulting from processes of hydrolysis and ion exchange which occur during the last period of utilization and the early step of the pedological period. Depending on the conservation conditions, a tertiary patina, formed as a consequence of processes of diffusion, mineralization, deposition, recrystallization, and monolithization, also appears [12-15].

Non-destructive techniques of analysis are important in order to preserve the patina of bronzes, not only because it can be an historical and archaeological value but also because the patina can be protective for the alloys under it. Accordingly, sampling the metal core of archaeological artifacts is in general not allowed so that the characterization of the metallic material aimed to identify its provenance and manufacturing technique has to be obtained from the physic-chemical properties of the metal patina [16-18].

In this context, solid state electrochemical techniques can provide a satisfying complement to other methodologies whose application on Cultural Heritage's field has been extended to a variety of materials [19,20]. The Voltammetry of Microparticles (VMP), a technique developed by Scholz et al. [21-23] based on the record of voltammetric response of a solid micro- or nanosample mechanically transferred to the surface of an inert electrode immersed into an appropriate electrolyte, is particularly suitable for archaeometric analysis because of its high inherent sensitivity [19-23]. Typical VMP experiments involve the abrasive attachment of minimal amounts of sample (at the microgram to nanogram, if necessary, level) and the application to archaeological objects is improved by using graphite pencil [24,25] and 'one-touch' sampling [26] that allows less invasiveness on the sample. The VMP has been applied to the study of copper/bronze archaeological objects [27,28] as well as their corrosion products [29-33] and application for mapping [34,35] authentication [36] and dating [37,38] purposes.

In this work VMP technique will be applied to 15 Roman bronze coins and one *Tessera* found in the south-west of Palatine, in the old rooms of the temple of *Magna Mater* in a complicated archaeological context distributed in five strata dated back between the second half of the 4th A.D. and the 20th century A.D. aiming at characterizing the patina and its corrosion products and evaluating the possible existence of different types of coins, especially for age and/or provenance and/or stratigraphy. In order to achieve these objectives, VMP was complemented with Electrochemical Impedance Spectroscopy (EIS) and Raman spectroscopy. EIS is a technique widely

used in metal corrosion studies, providing a good account of the growth of the passive films on metal surfaces, as recently reviewed [39]. EIS has been applied to archaeological metal [40] and that different equivalent circuits can be used for modeling experimental data [41-43]. Here, we used a cell adapted for testing coins and other metallic objects which are immersed into mineral water, a procedure recommended ensuring their morphological, structural and chemical integrity of the objects [44], and applying a bias potential for the reduction of dissolved oxygen acting as a redox probe, as previously described [45-47]. The essential idea is that the VMP and EIS responses are dependent on the composition of the base metal, its minting process and the 'corrosion history' of the object and that, under favorable conditions, electrochemical features can provide information for tracing the provenance and archaeological context of the same.

Experimental

Electrochemical instrumentation and procedures

Voltammetry of microparticles experiments were performed at sample-modified paraffin-impregnated graphite electrodes using commercial graphite bars (Staedtler Mars 200 HB, 2.0 mm diameter) using either 0.25 M HAc/NaAc buffer at pH 4.75 or 0.10 M $HClO_4$ aqueous solutions as supporting electrolytes. All electrochemical measurements were carried out using a CH I660 potentiostat. A standard three-electrode arrangement was used with a platinum auxiliary electrode and a Ag/AgCl (3M NaCl) reference electrode. EIS experiments were performed in mineral water from Bejís (Comunitat Valenciana, Spain) using a modified cell, adapted for partial immersion of metallic objects, already described [38]. Spectra were recorded in the 0.1 to 100000 Hz frequency range with amplitudes between 2 and 10 mV at different potentials between +1.00 and -1.00 V upon partial immersion of the archaeological piece into the electrolyte. For this aim, the coins used for calibration purposes were suspended from an insulating tong and immersed to a certain depth and served as a working electrode upon connection to a conventional crocodile clamp. For each piece, experiments were performed for three different immersion depths and varying the position of the clamp but maintaining an immersed area of ca. 1 cm^2. Three repeated experiments were performed for each one of these (depth plus clamp position) configurations. Prior to each EIS experiment, an equilibration time of 10 min was taken. Air-saturated mineral water from Bejís (Valencian Community, Spain) was used (Composition: dry residual 159 mg/L, HCO_3^-: 163 mg/L, SO_4^{2-}: 16 mg/L, Cl^-: mg/L, SiO_2: 4.3 mg/L, Ca^{2+}: 47 mg/L, Mg^{2+}: 6.2 mg/L, Na^+: 2.8 mg/L. Reference materials were Cu_2O and CuO chemical reagents (Carlo Erba), malachite, atacamite and brochantite minerals (Minerales de Colección, Almuñécar, Spain and Minerales de Torres, Villaviciosa de Odón, Spain).

Raman spectra of different coins were obtained by means of a XPlora Horiba MTB model and a 532 nm laser as excitation with maximum power of 90 mW. The samples were measured in backscattering geometry at room temperature. A 100 confocal microscope objective was used to focus the excitation laser on the sample and collect the scattered light to the spectrometer. More than 3 different areas were analyzed per sample, to obtain representative results. Exposure time, number of acquisitions and laser power varied among 5 – 20 s, 10 – 50 and 30 – 80 mW, respectively. Data acquisition was carried out with the LabSpec 6 Spectroscopy Suite from Horiba MTB.

The microstructure of coins was determined using field emission scanning electron microscopy (Model S-4800, Hitachi Ltd., Tokyo, Japan) operating at 20 kV. The microanalysis of samples was performed with X-ray microanalysis system (SEM/EDX). Photographic images of coins were carried out with a Leica M165 stereo microscope using a capture system of high resolution digital image IC80HD controlled by LAS program.

Samples

A series of 15 Roman coins (catalogue numbers 7464, 7561, 8934, 8935, 8956, 8959, 550588, 550590, 550592, 550595, 550597, 550600, 550610, 550612 and 550615) and a *Tessera* (catalogue number 550581) found in the old rooms of the temple of *Magna Mater*, located in the south-west of Palatine (Rome, Italy) were studied here. The excavation of *Soprintendenza Speciale per il Colosseo, il Museo nazionale Romano e l'Area Archeologica di Roma* found a large number of coins and other valuable objects (metal, ceramics and stones) assignable to daily life contests. In particular, the coins, where unearthed in a *latrina*, located on the south side of the *domus Tiberiana*, in a context dated between the second half and the end of the 4th century A.D, distributed into five strata: A: third and fourth quarter of the 5th century A.D.; B: 15th – 17th century A.D.; C: end of 15th century A.D. and 17th century A.D.; D: 18th – 20th century A.D. and E: uncertain dating. A simplified scheme of the complex strata configuration is depicted in Figure 1.

The *Magna Mater* Temple, dedicated to the Phrygian divinity Cybele, was inaugurated in 191 B.C. Lately it was destroyed by fire twice and rebuilt by Augusto in 3 A.D. The site, after the temporary abandonment in 410 A.D., was reused until the 17th century A.D. These findings, together with the stratigraphy, have contributed to the elaboration of a coherent periodization aimed at establishing timelines, original usage, changes and final destination of the site in which the coins were found. In particular, the coins of the *Magna Mater* Temple cover the entire Imperial Roman period, being of great importance for the history of the site and for the historical questions related to the reuse of the materials.

In fact, regarding to the stratigraphy of the site, the coins resulted oldest than the deposition's date, gathering around the first half of the 4th century (kingdom of Costanzo II, Valentiniano and Valente). The archaeologists explain that with a prolonged use of the Roman emissions [48] because the coins don't stop to circulate after the collapse of the Western Roman Empire and, considering the lack of the numismatic documentation of the first period of the high Middle Age, it is possible to suppose that these coins were the only ones available on monetary circulation.

Regarding the nominal analysis, with very few exceptions, the considered coins are *Aes* 3 and 4 which were the working capital of the Late Antiquity. These coins were common during the 4th century A.D. and still circulating during the last part of the 5th century A.D, under the Emperors of Costanzo II (337-361 A.D) and Graziano (colleague in the diarchy with Teodosio I), both of *Costantinidi* family [48]. In Table 1 the numismatic characterization, the mint and the stratigraphy of coins, are summarized.

Results and discussion

Organoleptic properties and corrosion products

The studied coins exhibited a relatively advanced state of corrosion, with a rough, irregular greenish layer covering in several cases almost entirely the base brownish surface. Figure 2 shows the Raman spectrum of sample 7464 for two different areas accompanied by a photographic image of that coin. The cuprite bands at 103, 151, 218, 420 and 630 cm^{-1} can be clearly seen in the area 1 [49,50]. Raman spectra permitted to identify cuprite and tenorite, is the case in the area 2 that it can distinguish tenorite bands at 290, 337 and 620 cm^{-1} [49,51] in the studied coins.

Figure 3 shows the a,b) SEM images and c,d) mapping of Cu and Pb of coins 8934 and 550615 where it can be observed the different surface microtexture and distribution of corrosion products of

such coins. The 8934 coin has a sharp and steep profile full of holes whereas in the case of coin 550615 the surface is much more smooth and little bored as can be seen on comparing Figures 3a,b. Significant differences also occur when mapping is done with the same coins (Figures 3c,d) in the areas previously observed. When the main components, copper and lead, are selected it can be noted that for the coin 8934 (Figure 3c) lead is found in relatively gross, localized areas whereas in the case of the coin 550615 (Figure 3d) lead is dispersed forming a fine deposit on the surface. The above cases represent the extreme types of SEM data, coins 7464, 8935, 8959 and 8956 being assigned to the 8934 type and coins 7561, 550581, 550588, 550590, 550592, 550595, 550597, 550600 and 550612 being similar to 550615. The elemental composition determined by EDX varied significantly from one region to another of the corrosion layers, the percentage of Cu ranging between 14 and 73 % (wt CuO) and the percentage of lead varying between 14 and 82 % (wt PbO_2), accompanied by variable amounts of Si, Ca, Sn and Al, as expected for bronze corrosion products accompanied by pedological deposits of calcite and/or clays.

Voltammetric pattern

The voltammetry of samples from the corrosion layers of the studied coins attached to graphite electrodes immersed into aqueous acetate buffer at pH 4.75 was dominated by cathodic signals at –0.10 V and –0.60 V vs. Ag/AgCl, corresponding, in agreement with reported data [31,33,38], to the reduction of cuprite and tenorite, respectively, to copper metal, processes widely described in literature [27-34]. The samples from the brownish region of the coins produce both peaks with different relative heights, thus suggesting that the above products are present in the metal patina. In positive-going potential scans (see Supplementary information), the voltammograms are dominated by a prominent anodic signal at ca. +0.05 V, corresponding to the stripping oxidation of the deposit of copper metal formed at more negative potentials. The voltammetry of the more corroded regions, of greenish hue, was similar, the signal at –0.10 V being increased. This feature can be attributed to the presence of other copper corrosion products (malachite, brochantite, atacamite, confirming data from Raman spectroscopy) whose reduction in acetate buffer occurs at ca. –0.10 V [31,33,38].

The voltammetric response in 0.10 M $HClO_4$, however, revealed significant differences in the voltammetric pattern of the different coins. Figure 4 shows the corresponding SWVs of samples from the brownish region of a corroded eurocent coin (a) and samples 8934 (b), 7464 (c) and 550615 (d). In such voltammograms, three cathodic peaks appeared at +0.50 (I), –0.05 (II) and ca.–0.40 V (III), often accompanied by an additional cathodic signal at ca. .–0.55 V (IV). The two first signals can be attributed to the proton-assisted reduction of cuprite materials having different shape and size distribution of the mineral particles, as suggested by the observation that the voltammograms of samples from eurocents, where the cuprite patina is expected to form a continuous, finely crystallized layer over the metal surface, displayed the first peak clearly enhanced relative to the two others. On the basis of the description of copper/bronze corrosion from Robbiola et al. [15,16], the signal I would be attributable to the reduction of cuprite forming the primary, continuous-like patina while the signal II would correspond to the reduction of cuprite forming a ‘porous’ secondary patina. The signal III can be unambiguously assigned to the reduction of tenorite, as denoted by blank experiments on microparticulate deposits of CuO whereas the signal IV can be attributed to the reduction of lead corrosion products, as confirmed by the appearance in positive-going potential scan voltammograms (see Figure 5) of a tall, stripping peak (IV’) corresponding to the oxidative dissolution of lead [36,37]. Such voltammograms are dominated by the oxidative dissolution of copper which frequently appears resolved into two separate signals at +0.20 and 0.00 V (II’). This response can be attributed to the oxidative dissolution of different deposits of metallic copper, a frequent situation in the voltammetry of

several metallic compounds [51-53], here resulting from the superposition of the oxidation of the base metal and/or that formed in the electrochemical reduction of the copper corrosion products.

This voltammetry can be described in terms of the presence of cuprite and tenorite as a main copper corrosion products accompanied by some amount of lead corrosion products. It is pertinent to note, however, that prolonged corrosion of lead-containing bronze objects lead to an increase of the lead corrosion products/copper corrosion products ratio, so that the proportion of lead in the base metal alloy can be overestimated from voltammetric data [55].

In order to use voltammetric data for archaeometric purposes, it has to be noted that the abrasive method used for sampling involves the possibility of deposition of 'external' materials (dust, etc.) existing in the corrosion layer as a result of pedological processes and/or environmental contamination, with the concomitant influence in the recorded electrochemical response. These effects would be possibly minimally influential in our case because: i) sampling was performed on selected, 'clean' locations of the coins; ii) under our experimental conditions, most of the components of 'external' materials (clays, calcareous minerals) are electrochemically silent. In fact, when sampling on the greenish regions of all coins, the voltammograms were essentially identical, as shown in Figure 6. These features suggested that, although when 'advanced' corrosion occurs, the composition of the external corrosion layers (dominated by green products of the atacamite, brochantite and malachite mineral families) and hence the corresponding voltammetric response becomes essentially identical for all coins, thus suggesting that such response reflects basically the common 'corrosion history' of the coins, consistently with the archaeological context. In contrast, when sampling was carried out in the regions where the primary patina was exposed, the voltammetric response differs clearly from one to another coin. As far as it seems reasonable to expect that this primary patina was sensitive to the composition of the base alloy and the peculiarities of the minting process, the observed differences could be attributed to different monetary origins.

Accordingly, grouping of coins was based on the peak current ($i(E)$) ratios between the different voltammetric signals (I-III) recorded under fixed electrochemical conditions. Figure 7 depicts the two-dimensional diagram of the ratios i(III)/i(I) and i(II)/i(I) from SWV voltammograms of sample-modified graphite electrodes in contact with 0.10 M $HClO_4$. The first ratio can be considered as representative of the tenorite/cuprite ratio whereas the second would be representative of the ratio between the cuprite forming the secondary and primary patinas, respectively. The double logarithmic representation permitted to discern between a group of samples with high tenorite to cuprite content (8934, 8935 and 8959 coins) from a second with lower relative content of tenorite (7464, 7561 and 8956) and a third group dominated by the peak at +0.50 V (all other samples).

EIS data

In order to test the possibility of an electrochemical grouping of coins, EIS experiments were performed using the modified cell, adapted for partial immersion of metallic objects previously described [38]. Air-saturated mineral water was employed in order to combine: i) minimal degradation of the coins [44] and ii) use of the reduction of dissolved oxygen as a redox probe [45-47]. Replicate experiments provided excellent repeatability in the frequency (f) range between 10^5 and 0.10 Hz, but the response was increasingly erratic on decreasing frequency below this last value. Attempts to perform EIS measurements on two coins (8956 and 550588) were unsuccessful due to the extension of the corrosion deposits so that no effective clamping was carried out.

Figure 8 compares the EIS spectra for coins a) 550612, b) 550600, c) 550597 and d) 550592 under the aforementioned conditions. The Nyquist representation of the imaginary (Z_{imag}) vs. the real (Z_{real}) components of the impedance consisted apparently of two more or less overlapping capacitive loops. These spectra were modeled using simple circuits similar to those used in different cases of metal corrosion [39-46] upon considering that the metal nucleus is covered by a fine layer of continuous primary patina of cuprite eventually covered by a porous, permeable secondary corrosion patina [15,16]. In the case of moderate corrosion, experimental data can be fitted to a circuit (Figure 9a) based on the elements of a Randless circuit: a solution resistance (R_s) combined with a series association of a charge transfer resistance at solid/electrolyte interface (R_{ct}) in parallel with the interfacial, double-layer capacitance of that interface, Q_{dl}, adding a parallel combination of a resistance (R_{corr}) and a capacitive element (Q_{corr}) representative of the resistance and charge separation at the gross corrosion layer. The capacitive elements were modeled using constant phase elements (CPEs) for accounting the non-ideality of the represented interfaces. This model provided in general a reasonable agreement with experimental data (see Figure 8), although in several cases the fit was increased using an equivalent circuit including a second parallel combination of resistance (R_{porous}) and CPE (Q_{porous}) representative of the ohmic resistance and charge separation in the porous secondary patina (see Figure 9b). For reasons of simplicity, in the following the EIS parameters resulting from the fit of experimental data to the equivalent circuit in Figure 9a were used.

Table 2 summarizes the values of the average values of the impedance parameters from three independent experimental spectra using the equivalent circuit in Figure 9a for five of the studied coins. Although the geometrical area of the coin immersed into mineral water was the same within ±20%, differences in effective area may be larger thus making difficult the comparison between the EIS parameters for different coins. To compensate this effect, the variation of the different individual impedances on the logarithm of the absolute value of the impedance at the lowest studied frequency (Z_{low}) was studied. Figure 10a shows the plot of experimental values of $\log R_{ct}$ vs. $\log|Z_{low}|$ for the coins of the first and second VMP groups (7464, 8934, 8935, 8959) using forced fitting to the equivalent circuit in Figure 9a (data for three independent EIS spectra for each coin are taken). This second quantity is approximately representative of the total ohmic resistance of the system and can be used as a normalization factor for EIS experiments in irregular surfaces [45-47]. One can see here that all data points fall in a common curved path, thus suggesting that there is a common EIS behavior. In contrast, if the representation of $\log R_{corr}$ vs. $\log|Z_{low}|$ is extended to all studied coins (Figure 10b), the data points of the third VMP group of coins fall in a different, almost linear path.

These features suggest that grouping of coins from VMP and EIS data, recorded under clearly different experimental conditions, was consistent. Interestingly, EIS data can provide an additional, fine grouping of the coins. Thus, Figure 11 depicts the variation of R_{corr} on R_{ct} , determined by fitting of experimental EIS data to the equivalent circuit in Figure 9a for the studied coins (average values from three independent replicate experiments for each coin are represented). The resulting two-dimensional diagram provides a reasonable separation between the points representative of the first (8934 and 8935 coins) and second (7464, 8959) VMP groups and those of the third VMP group which here can be resolved into two clearly separated sub-groups, one composed by coins 550612 and 550615 and the other constituted by coins 550592, 550595, 550597, 550600 and 550610.

Discussion

The variation of peak current ratios in VMP experiments in Figure 7 can be rationalized on the basis of the previous modeling of corrosion of silver coins [56], assuming that long-term corrosion process in terms of a kinetic equation of the type:

$$\frac{dx}{dt} = Kx^{-\delta} \quad (1)$$

where x represents the amount (mass, mole number) of metal by surface unit corroded during the corrosion process and K a rate constant [57]. This last is representative of the rate of metal deterioration which depends on environmental corrosivity [58]. Integration of the above equation leads to:

$$x = [x_o^{1+\delta} + (1+\delta)Kt]^{\frac{1}{1+\delta}} \quad (2)$$

Assuming (roughly) that similar rate equations are applicable to describe the growth of the secondary corrosion products (for both the situations represented in Figures 8a and 8b) and that the peak currents recorded in VMP experiments are proportional to the amount of the respective corrosion products (peak I: primary cuprite patina; peak II: secondary cuprite patina; peak III: tenorite in the secondary patina), eliminating the time between the corresponding rate equations, yields to an equation of the form [56]:

$$\frac{i(\mathrm{III})}{i(\mathrm{I})} = A + B\left(\frac{i(\mathrm{II})}{i(\mathrm{I})}\right)^{\alpha} \quad (3)$$

where A and B represent numerical coefficients whose value depends on the electrochemical conditions (potential scan rate, etc.) the rate constants and exponents of the potential rate laws (δ exponents in equations such as Eq. (2) for the different interconversion processes) and the initial amount of the primary and secondary patinas when the formation of secondary and ternary corrosion products starts. The exponent α depends on the aforementioned δ exponents and should be, under ordinary corrosion conditions, close to one. Since electrochemical corrosion operating under burial conditions proceeds via local cells [58], the peak currents in VMP experiments, which are representative of relatively small areas of the objects, could vary significantly from one coin to another, thus yielding different individual values of the i(III)/i(I) and i(II)/i(I) ratios. However, different coins having the same metallurgical properties (composition of the base metal, minting process) and essentially identical 'corrosion history' should fall within the same i(III)/i(I) vs. i(II)/i(I) line. Expected linear variations of log[i(III)/i(I)] on log[i(II)/i(I)] are superimposed to experimental data points in Figure 7. Although there is large data dispersion, tendency lines can be considered reasonably consistent with the proposed grouping of the coins.

To interpret EIS data, one can assume that a continuous primary patina is always formed. Assuming homogeneity of this patina, its resistance by surface area unit at a corrosion time t would be:

$$R_{\mathrm{pp}}(t) = \delta_{pp}(t)/\sigma_{\mathrm{pp}} \quad (4)$$

where $\delta_{\mathrm{pp}}(t)$ represents the thickness of the corrosion layer σ_{pp} the conductivity, assumed to be constant. In turn, the resistance associated to the secondary patina should account for the contribution of the electrolyte filling the pores. Then, introducing the fraction of covered surface area, θ_{sp}, and the porosity, χ_{sp} [59], one can write [47]:

$$R_{sp}(t) = \frac{\delta_{\mathrm{sp}}(t)}{\vartheta_{sp}(t)}\{\frac{\chi_{sp}(t)}{\sigma_{sp}} + \frac{[1-\chi_{sp}(t)]}{\sigma_{el}}\} \qquad (5)$$

where σ_{el} and σ_{pp} denote the electrolyte and secondary patina conductivities, respectively, and $\delta_{\mathrm{pp}}(t)$ represents the thickness of the corrosion layer. Assuming that the degree of coverage and porosity remain time-independent, the increase of the thickness of the primary and secondary patina with corrosion time should satisfy a potential rate law [47] so that:

$$R_{\mathrm{pp}}(t) = C + D[(1+\beta)t]^{\frac{1}{1+\beta}} \qquad (6)$$

$$R_{sp}(t) = F + G[(1+\gamma)t]^{\frac{1}{1+\gamma}} \qquad (7)$$

Here, *C*, *D*, *F*, and *G* represent time-independent coefficients depending on the aforementioned conductivities, porosity and surface coverage and, as before, on the initial amount of primary patina at the beginning of the process of formation of secondary patina. Assuming that the exponents β and γ are quite similar, a reasonable hypothesis based on data on lead [37,45,57] and copper corrosion [38,47], eliminating time between the above equations leads to predict linear dependences between R_{sp} and R_{pp} and between those quantities and the total impedance at low frequencies, roughly taken as the sum of the same:

$$R_{\mathrm{sp}}(t) \propto R_{\mathrm{pp}} \qquad (8)$$

$$R_{\mathrm{sp}} \propto \left|Z_{\mathrm{low}}(t)\right| \quad (\approx R_{\mathrm{pp}}(t) + R_{\mathrm{sp}}(t)) \qquad (9)$$

These predictions agree with the results in Figure 11. Again, as the corrosion conditions of the individual coins can vary, the individual values of R_{pp}, R_{sp} and Z_{low} can vary from one coin to another, but such values should be confined to common linear variations. This is just the result when experimental data are represented (Figures 10 and 11), thus suggesting that differences between different linear paths can be attributed to differences in the 'intrinsic' properties (alloy composition, minting technique, provenance) of the coins. Accordingly, electrochemical grouping of coins appears to be a judicious option under our archaeological (a set of coins from the same archaeological context) and experimental conditions (common VMP and EIS experimentation).

The high percentage in Pb given by the surface analysis is consistent with the use of lead in the ancient Rome, especially during the IIIth and IVth century [60-61]. Moreover, the percentage of lead in the coins is strictly related to the economic issues of the period. Copper and tin were available only in certain regions of the Empire, for example in Britain, *Lusitania* or *Gallecia* [62]. The lost of the control over these regions meant the loosing of the tin mine as happened in Salamanca in the fifth century during the German invasion [62].

Numismatic features indicated that the majority of the Roman bronze coins here studied were minted between the second half of the 4th and the end of the 5th century A.D and, after the falling of the Western Roman Empire they continued to circulate until the Middle Ages. For this reason these coins were found at different stratigraphic levels, supporting the hypothesis that they represented the only coinage available on the market. Moreover, the lacking of numismatic documentation for Medieval Age further supported this archaeological reconstruction. Four coins (8935, 8935, 8956 and 8959), all found in the level E, were minted between 6th and 4th B.C.

Between the 5th and 7th centuries Rome had an important monetary system of exchange, circulation and transition of previously minted coins as confirmed by the stratigraphy of the *Magna Mater* Temple. Although the mint of Rome was the most important of the Empire, numerous oriental mints were also active and found in the context of *Magna Mater*. The reform of Diocleziano was aimed to an economic and administrative decentralization of the Empire; lately, under the leadership of Costantino, the oriental mints became the most important and the others (e.g., London mint) were dismantled. The crisis and the fall of some regions of the Empire resulted in the loss of several sourcing areas of raw materials (e.g., Sn deposits of Britain), essential for the coinage of bronze coins. However, lead, the metal *par excellence* of the Romans, remained the most common metal in the Mediterranean area due to the occurrence of numerous Pb-deposits in the ancient Roman world. Also the easy recast and reuse of Pb favoured its diffusion during the Late Empire, involving the production of Cu-Pb-Sn and Cu-Pb alloys employed for different purposes.

The grouping obtained by the electrochemical measurements is supported by the stratigraphic context of the *Magna Mater* site (see Figure 1) and can be summarized as:

a) Coins found in the stratigraphic level A (7464), dated back in 4th A.D. and 5th A.D. and coins from the level E minted between 6th B.C. and 4th B.C., formed a well-defined group although sub-divided into two sub-groups (8934 and 8935, and 7464, 7561, 8956 and 8959, respectively). All these coins undergo presumably prolonged corrosion and their possible reutilization would be confined to the 5th A.D. century.

b) The other group of coins was electrochemically distributed within the different stratigraphic levels. A first sub-group comprises the coins 550590, 550612 and 550615 (level D, 18th – 20th A.D. period), whereas the second includes the coins 550588, 550592, 550600 and 550610 (level C) and 550595 and 550597 (level B) all found in strata dated back in the 15th – 17th A.D. period, thus suggesting a reuse of such coins in mediaeval times.

c) The *Tessera* (550581), although found in the level A, displayed an electrochemical response close to that of coins from the B, C, D levels. This discrepancy can in principle be attributed to differences between the conditions of aging of this decorative object relative to coins.

Conclusions

A series of 15 Roman coins and a *Tessera* found in the old rooms of the temple of *Magna Mater* (south-west of Palatine, Rome), dated back between the second half and the end of the 4th century A.D. but distributed through a complex stratigraphic context were studied using the voltammetry of microparticles methodology and electrochemical impedance spectroscopy aided by Raman spectroscopy and SEM/EDX. The corrosion products were mainly cuprite and tenorite, followed by lead corrosion compounds, the corrosion products of copper and lead were found in different proportions indicating a different corrosion history related to coins' stratigraphic position.

Characteristic voltammetric patterns of cuprite in the primary and secondary corrosion patina and tenorite in the secondary patina were recorded for submicrosamples of the corrosion layers of coins in contact with 0.10 M $HClO_4$. The ratios between different pairs of peak currents recorded under fixed electrochemical conditions were used for grouping the coin samples into three main groups, presumably corresponding to different coinages/provenances. This grouping was consistent with that established from EIS data obtained upon immersion of the coins in air-saturated mineral water and using the reduction of dissolved oxygen as a redox probe. This second methodology permitted a subsequent fine grouping of the coins.

In conclusion, the discrimination of the coins, which depends on their usage history, allows to grouping the samples on the basis of their occurrence in the stratigraphic sequence of the archaeological site. Taking into account the highly non-destructive and non-invasive characteristics of the proposed electrochemical methodologies, this approach can be a useful tool for archaeologists in the future.

Ackonwledgements: Financial support from the MINECO Project CTQ2014-53736-C3-2-P which is supported with ERDF funds is gratefully acknowledged. PhD grants of the Department of Earth Sciences, Sapienza University of Rome, are gratefully thanked.

References

[1] D.A. Scott, *Metallography and Microstructure of Ancient and Historic Metals*, The Getty Conservation Institute, Paul Getty Museum, Malibu (1991).

[2] Dowsett, M. & Adriaens, A. The role of SIMS in cultural heritage studies. *Nucl. Instruments Methods Phys. Res. Sect. B Beam Interact. with Mater. Atoms* **226,** 38–52 (2004).

[3] Aucouturier, M. & Darque-Ceretti, E. Materials Surface Science Applied to the Investigation of Cultural Heritage Artefacts. *Procedia Mater. Sci.* **9,** 31–47 (2015).

[4] Bertolotti, G., Bersani, D., Lottici, P. P., Alesiani, M. & Malcherek, T. Micro-Raman study of copper hydroxychlorides and other corrosion products of bronze samples mimicking archaeological coins. 1451–1457 (2012). doi:10.1007/s00216-011-5268-9

[5] Buccolieri, G., Buccolieri, A., Donati, P., Marabelli, M. & Castellano, A. Portable EDXRF investigation of the patinas on the Riace Bronzes. *Nucl. Instruments Methods Phys. Res. Sect. B Beam Interact. with Mater. Atoms* **343,** 101–109 (2015).

[6] Budd, P.; Gale, D.; Pollard, A.M.; Thomas, R.G.; Williams, P.A. Evaluating lead isotope data: further observations, Archaeometry 1993, 35, 241-247.

[7] M. Milazzo, Radiation applications in art and archaeometry X-ray fluorescence applications to archaeometry. Possibility of obtaining non-destructive quantitative analyses, Nucl. Instr. Meth. Phys. Res. B 213 (2004) 683–692.

[8] R. Linke, M. Schreiner, Energy dispersive X-ray fluorescence analysis and X-Ray microanalysis of medieval silver coins: an analytical approach for nondestructive investigation of corroded metallic artifacts, Mikrochim. Acta 133 (2000) 165–170.

[9] R. Linke, M. Schreiner, G. Demortier, The application of photon, electron and proton induced X-ray analysis for the identification and characterization of medieval silver coins, Nucl. Instr. Meth. Phys. Res. B 226 (2004) 172–178.

[10] Attanasio, D., Bultrini, G., and Ingo, G. M. 2001, The possibility of provenancing a series of bronze punic coins found at Tharros (Western Sardinia) using the literature lead isotope database, *Archaeometry*, **43**, 529–47.

[11] Constantinides, I., Adriaens, A., and Adams, F., 2002, Surface characterization of artificial corrosion layers on copper alloy reference materials, *Applied Surface Science*, **189**, 90–101.

[12] Scott, D. A., 1994, An examination of the patina and corrosion morphology of some Roman bronzes, *Journal of the American Institute of Conservation*, **33**, 1–23.

[13] Robbiola, L., and Portier, R., 2006, A global approach to the authentication of ancient bronzes based on the characterization of the alloy–patina–environment system, *Journal of Cultural Heritage*, **7**, 1–12.

[14] Sandu, I., Marutoiu, C., Sandu, I. G., Alexandru, A., and Sandu, A. V., 2006, Authentication of Old Bronze Coins I. Study on Archaeological Patina, *Acta Universitatis Cibinensis Section F Chemia*, **9**, 39–53.

[15] Robbiola, L., Blengino, J. -M., and Fiaud, C., 1998, Morphology and mechanisms of formation of natural patinas on archaeological CuSn alloys, *Corrosion Science*, **40**, 2083–111.

[16] Robbiola, L., and Hurtel, L.- P., 1997, Standard nature of the passive layers of buried archaeological bronze - The example of two Roman half-length portraits, in MacLeod, I., Pennec, S., and Robbiola, L., Eds., METAL 95, James & James Science Publ., London, pp. 109–17.

[17] Wang, Q., and Merkel, J. F., 2001, Studies on the redeposition of copper in Jin bronzes from Tianma-Qucun, Shanxi, China, *Studies in Conservation*, **46**(4), 242-50.

[18] Welter, J.-M., 2003, The zinc content of brass: a chronological indicator, *Techné*, **18**, 27–36.

[19] Doménech-Carbó, A., Doménech-Carbó, M. T. & Costa, V. *Electrochemical Methods in Archaeometry, Conservation and Restoration*. (2009).

[20] Doménech-Carbó, A. Voltammetric methods applied to identification, speciation, and quantification of analytes from works of art: an overview. *J. Solid State Electrochem.* **14,** 363–379 (2010).

[21] F. Scholz, B. Meyer, *Electroanalytical Chemistry, A Series of Advances* vol. 20, 1 (1998).

[22] F. Scholz, U. Schröder, R. Gulabowski, A. Doménech-Carbó, *Electrochemistry of Immobilized Particles and Droplets*, 2nd edit. Springer, Berlin-Heidelberg (2014).

[23] Doménech-Carbó, A., Labuda, J., and Scholz, F., 2013, Electroanalytical chemistry for the analysis of solids: characterization and classification (IUPAC Technical Report), *Pure and Applied Che*mistry, **85**, 609–31.

[24] Blum, D., Leyffer, W. & Holze, R. Pencil-Leads as new electrodes for abrasive stripping voltammetry. *Electroanalysis* **8,** 296–297 (1996).

[25] V. Costa, F. Urban, Reviews in Conservation, International Institute of Conservation 2005, 6, 48.

[26] Doménech-Carbó, A., Doménech-Carbó, M. T., and Peiró-Ronda, M. A., 2011a, 'One-touch' voltammetry of microparticles for the identification of corrosion products in archaeological lead, *Electroanalysis*, **23**, 1391–1400.

[27] V. Costa, K. Leyssens, A. Adriaens, N. Richard, F. Scholz, *J. Solid State Electrochem.* **2010**, *14*, 449.

[28] F. Arjmand, A. Adriaens, *J. Solid State Electrochem*. **2012**, *16*, 535.

[29] Souissi, N., Bousselmi, L., Khosrof, S., and Triki, E., 2004, Voltammetric behaviour of an archeaological bronze alloy in aqueous chloride media, *Materials and Corrosion*, **55**, 284–92.

[30] Serghini-Idrissi, M., Bernard, M.C., Harrif, F.Z., Joiret, S., Rahmouni, K., Srhiri, A., Takenouti, H., Vivier, V., and Ziani, M., 2005, Electrochemical and spectroscopic characterizations of patinas formed on an archaeological bronze coin, *Electrochimica Acta*, **50**, 4699–709.

[31] Doménech-Carbó, A., Doménech-Carbó, M. T., and Martínez-Lázaro, I., 2008, Electrochemical identification of bronze corrosion products in archaeological artefacts. A case study. *Microchimica Acta*, **162**, 351–9.

[32] Satovic, D., Martinez, S., and Bobrowski, A., 2010, Electrochemical identification of corrosion products on historical and archaeological bronzes using the voltammetry of micro-particles attached to a carbon paste electrode, *Talanta*, **81**, 1760–5.

[33] Doménech-Carbó, A., Doménech-Carbó, M. T., Redondo-Marugán, J., Osete-Cortina, L., and Vivancos-Ramón, M. V., 2015, Electrochemical characterization of corrosion products in leaded bronze sculptures considering ohmic drop effects on Tafel analysis, *Electroanalysis*, 28, 833 (2016).

[34] Doménech-Carbó, A., Doménech-Carbó, M. T., and Martínez-Lázaro, I., 2010, Layer-by-layer identification of copper alteration products in metallic works of art using the voltammetry of microparticles approach, *Analytica Chimica Acta* **610**, 1–9.

[35] Doménech, A., Rodríguez, F. & Osete, L. Mapping of corrosion products of highly altered archeological iron using voltammetry of microparticles. *Microchem. J.* **106,** 41–50 (2013).

[36] Doménech-Carbó, A., Doménech-Carbó, M. T., Peiró-Ronda, M. A., and Osete-Cortina, L., 2011b. Authentication of archaeological lead artifacts using voltammetry of microparticles: the case of the *Tossal de Sant Miquel* Iberian plate, *Archaeometry*, **53**, 1193–211.

[37] Doménech-Carbó, A., Doménech-Carbó, M. T., and Peiró-Ronda, M. A., 2011, Dating archaeological lead artifacts from measurement of the corrosion content using the voltammetry of microparticles, *Analytical Chemistry*, **83**, 5639–44.

[38] Doménech-Carbó, A., Doménech-Carbó, M. T., Capelo, S.; Pasíes, T., and Martínez-Lázaro, I., 2014, Dating archaeological copper/bronze artifacts using the voltammetry of microparticles, *Angewandte Chemie International Edition*, **53**, 9262–6.

[39] D.D. Macdonald, *Electrochim. Acta* **2011**, *56*, 1761.

[40] Cano E, Lafuente D, Bastidas DM (2010) J Solid State Electrochem 14:381-391.

[41] W.S. Li, S.Q. Cai, J.L. Luo, *J. Electrochem. Soc*. **2004**, *151*, B220.

[42] W. Liu, H. Zhang, Z. Qu, Y. Zhang, J. Li, *J. Solid State Electrochem*. **2010**, *14*, 965.

[43] L.A. Toledo-Martos, M.A. Pech-Canul, *J. Solid State Electrochem*. **2011**, *15*, 1927.

[44] C. DeGrigny, G. Guibert, S. Ramseyer, G. Rapp, A. Tarchini, *J. Solid State Electrochem*. **2010**, *14*, 425.

[45] A. Doménech-Carbó, M.T. Doménech-Carbó, M.A. Peiró-Ronda, I. Martínez-Lázaro, J. Barrio, *J. Solid State Electrochem*. **2012**, *16*, 2349.

[46] A. Doménech-Carbó, M. Lastras, F. Rodríguez, L. Osete-Cortina, *J. Solid State Electrochem*. **2014**, *18*, 399.

[47] A. Doménech-Carbó, S. Capelo, J. Piquero, M.T. Doménech-Carbó, J. Barrio, A, Fuentes, W. Al-Sekkaneh. 2016. Dating archaeological copper using electrochemical impedance spectroscopy. Comparison with voltammetry of microparticles dating. *Materials and Corrosion*, vol. 67, pp. 120-129.

[48] F. Coletti, L'obolo della dea: monete dai contesti di vita, abbandono e distruzione dell'area sud ovest del Palatino, Soprintendenza Speciale per il Colosseo, il Museo Nazionale Romano e l'Area Archeologica di Roma

[49] L. Burgio, R.J.H. Clark, Library of FT-Raman spectra of pigments, minerals, pigment media and varnishes, and supplement to existing library of Raman spectra of pigments with visible excitation. Spectrochim. Acta A 57 (2001) 1491-1521.

[50] Ł. Ciupiński, E. Fortuna-Zaleśna, H. Garbacz, A. Koss, K.J. Kurzydłowski, J. Marczak, J. Mróz, T. Onyszczuk, A. Rycyk, A. Sarzyński, W. Skrzeczanowski, M. Strzelec, A. Zatorska, G.Z. Żukowska, Comparative Laser Spectroscopy Diagnostics for Ancient Metallic Artefacts Exposed to Environmental Pollution. Sensors 10 (2010) 4926-4949.

[51] R. Linke, M.A. Ziemann, The Detection of Copper-based Pigment Darkening by Biuret-reaction in Mural Paintings by SEM-EDX, Micro-XRF and micro-Raman Spectroscopy. Int. J. Cons. Sci. 5 (2014) 129-136.

[52] N. Zakharchuk, S. Meyer, B. Lange, F. Scholz, A Comparative Study of Lead Oxide Modified Graphite Paste Electrodes and Solid Graphite Electrodes with Mechanically Immobilized Lead Oxides, Croat. Chem. Acta 73 (2000) 667–704.

[53] S. Komorsky-Lovric, M. Lovric, A.M. Bond, Comparison of the square-wave stripping voltammetry of lead and mercury following their electrochemical or abrasive deposition onto a paraffin impregnated graphite electrode, Anal. Chim. Acta. 258 (1992) 299–305.

[54] M. De Keersmaecker, M. Dowsett, R. Grayburn, D. Banerjee, A. Adriaens, In-situ spectroelectrochemical characterization of the electrochemical growth and breakdown of a lead dodecanoate coating on a lead substrate, Talanta. 132 (2015) 760–768.

[55] A. Doménech-Carbó, M.T. Doménech-Carbó, J. Redondo-Marugán, L. osete-Cortina, J. barrio, A. Fuentes, M.N. Vivancos-Ramón, W. Al-Sekkaneh, I. Martínez-Lázaro, T. Pasíes, Electrochemical characterization and dating of archeological leaded bronze objects using the voltammetry of immobilized particles, submitted.

[56] A. Doménech-Carbó, M.T. Doménech-Carbó, Pasíes, T.; Bouzas, M.C. 2012. Modeling corrosion of archaeological silver-copper coins using the voltammetry of immobilized particles. *Electroanalysis*, 24, 1945-1955.

[57] S. Reich, G. Leitus, S. Shalev, *New J. Phys*. **2003**, *5*, 99.1.

[58] L.L. Sheir, R.A. Jarman, G.T. Burstein, *Corrosion. Metal/Environment Reaction*, vol. 1, 3rd ed., Butterworth Heinemann, Great Britain, 1998. Chapter 2, pp. 2-5, 2-73.

[59] G. Chen, C.C. Waraksa, H. Cho, D.D. Macdonald, T.E. Mallouk, TE EIS Studies of Porous Oxygen Electrodes with Discrete Particles. I. Impedance of Oxide Catalyst Supports. J. Electrochem. Soc. 150 (2003) E423–E428.

[60] I. Calliari, M. Magrini, A. Zambon, P. Guerriero, R. Martini. Microstructural and Compositional Characterization of Roman Coins, X-Ray Spectrometry 28, 86-90 (1999).

[61] M. Scuotto, C. Bassi, M. Lezzerini, E. Grifoni, S. Legnaiolom G. Lorenzetti, S. Pagnotta, V. Palleschi. X-Ray fluorescence analysis on a group of coins from the ancient roman city of Tridentum (Trento, Italy), X-Ray Spectrometry 2014, 43, 370-374.

[62] J.C. Edmonson, Mining in the Later Roman Empire and beyond: continuity or disruption?. The Journal of the Roman Studies, Vol.79 (1989) pp. 84-102.

Table 1. Numismatic characterization and features of the coins.

Sample	Value	Mint	Age	Context ([a])	Issuing authorities	g	mm
Nr. Inv. 550615 TMM 94 RZ 0 s.f. 350	Dupondio, OR	Rome	85 A.D. Domiziano (71-92 A.D.)	D	D/ [IMP CAES DOMIT AVG GERM COS XI CENS POT] R/ [FORTVN]AE AVGVSTI; S C RIC II, 191, n. 293	7.55	29-30
Nr. Inv TMM 98 RZ 5658 s.f. 7464	Aes 3, MI	not id.	Valente (364-378 A.D.)	A	D/ DN VA[LEN S PF AVG] R/ [SE]CVR[RITAS REIPVBLICAE] LRBC II, 61, n. 739.	1.37	14
Nr. Inv. 550588 TMM 94 RZ 4448 s.f. 754	Aes 3, MI	Siscia	Costanzo II (346-350 A.D.)	C	D/ [DN CONSTANT IVS PF AVG] R/ FEL[TEMP REPARATIO] LRBC II, 69, n. 1115.	1.7	15-16
Nr. Inv. 550612 TMM 94 RZ 0 s.f. 334	Aes 3, MI	Tessalonica	Costanzo II (375-378 A.D.)	D	D/ DN VALENS [PF]AVG R/ SECVRITAS [REIPVBLICAE]; ●; CONSA	2.2	18
Nr. Inv. 550600 TMM 94 RZ 4451 s.f. 4430	Aes 3, MI	not id.	Graziano (367-378 A.D.)	C	D/ [DNGRA]TIA NVSPFAVG R/ [GLORIA ROMANORVM] LRBC II, 68, n. 1072	1.15	13
Nr. Inv. 550597 TMM 94 RZ 4451 s.f. 787	Aes 3, MI	Sciscia	Costanzo II (346-350 A.D.)	B	D/ DNCONSTAN TIVS[PF]AVG R/ [FELTEMP] REPARATIO; R●M●S	1.79	17.5
Nr. Inv. 550610 TMM 94 RZ 4482 s.f. 748	Aes 3	not id.	IV-VI century A.D.	C	not id.	1.11	14
Nr. Inv. 550581 TMM 94 RZ 4445 s.f. 554.	Tessera ([b])	not id.	not id.	A	not id.	1.12	15
Nr. Inv. 550592 TMM 94 RZ 4451 s.f. 406	Aes 4	not id.	375-378 A.D.	C	D/ [DN VALEN S PF AVG] R/ [VICTORIA AVGGG]	1.13	10.1
Nr. Inv 550590 TMM 94 RZ 4451 s.f. 398	Aes 2	not id.	not id.	D	not id.	3.5	23-24
Nr. Inv. 550595 TMM 94 RZ 4451 s.f. 428	Aes 3	not id.	not id.	B	D/ [DN VALEN S PF AVG] R/ GLO[RIA RO MANORVM]	1.28	15
Nr. Inv TMM 99 RZ5814 s.f. 7561	n.d.	not id.	not id.	E	not id.	1.2	13
Nr. Inv . TMM 07 RZ 3758 s.f. 8956	Aes 4	not id.	IV and VI century B.C.	E	not id.	1	10.3
Nr. Inv TMM 07 RZ 6708 s.f. 8934	Aes 4	not id.	IV and VI century B.C.	E	not id.	1	11
Nr. Inv TMM 07 RZ 6708 s.f. 8935	Aes 4	not id.	IV and VI century B.C.	E	not id.	1	11
Nr. Inv TMM 07 RZ 6720 s.f. 8959	Aes 4	not id.	IV and VI century B.C.	E	not id.	1	13.5

([a]): A = third and fourth quarter of the V century A.D.; B = XV-XVII century A.D.; C = end of XV century and XVII century A.D.; D = XVIII-XX century A.D.; E = uncertain

([b]): Presumably the object was identified as some kind of token of personal use that allowed to benefits of the services in the commercial district of the Magna Mater.

Table 2. Values of the circuit elements used to model EIS spectra of the studied coins. Average values from fitting of circuits in Figure 8 to three independent experimental spectra in conditions such as in Figure 7.

Coin	R_s (Ω)	R_{ct} (kΩ)	Q_{dl} (μF $s^{-(1-n1)}$)	n_{dl}	R_{corr} (kΩ)	Q_{corr} (μF $s^{-(1-n1)}$)	n_{corr}
7464	20±10	73±3	2.63±0.05		120±40	7.5±0.2	
8934	30±10	44±2	1.44±0.05		63±2	0.12±0.05	
8935	20±10	28.1±0.5	3.6±0.2		16.7±0.6	1.66±0.02	
8959	20±10	24.8±0.4	12.6±0.2		5.7±0.2	0.64±0.02	
550615	220±10	5.1±0.3	130±4		2.1±0.3	0.55±0.05	

Figures

Figure 1. Scheme of strata distribution in the *Magna Mater* archaeological site.

Figure 2. Raman spectrum and photographic image of coin 7464 (• is cuprite Cu_2O bands and ♦ is tenorite CuO bands).

Figure 3. a,b) SEM images and c,d) Cu plus Pb mapping of coins a,c) 8934 and b,d) 550615.

Figure 4. SWVs of samples from the brownish region of: a) corroded eurocent (5 cts coin) and samples b) 8934, c) 7464 and d) 550615 attached to graphite electrodes immersed into 0.10 M $HClO_4$ aqueous solution. Potential scan initiated at +0.75 V in the negative direction; potential step increment 4 mV; square wave amplitude 25 mV; frequency 5 Hz. Two or three replicate measurements on different areas of the coin surface are superimposed.

Figure 5. SWVs of samples from the brownish region of samples: a) 8934, b) 7464 and c) 550615 attached to graphite electrodes immersed into 0.10 M $HClO_4$ aqueous solution. Potential scan initiated at –0.75 V in the positive direction; potential step increment 4 mV; square wave amplitude 25 mV; frequency 5 Hz. Three replicate measurements on different areas of the coin surface are superimposed.

Figure 6. SWVs of samples from the greenish region of coins in this study attached to graphite electrodes immersed into 0.10 M $HClO_4$ aqueous solution. Potential scan initiated at +0.75 V in the negative direction; potential step increment 4 mV; square wave amplitude 25 mV; frequency 5 Hz.

Figure 7. Two-dimensional diagram in double logarithmic scale representing the ratios i(III)/i(I) and i(II)/i(I) from SWV voltammograms of sample-modified graphite electrodes in contact with 0.10 M $HClO_4$. Conditions such as in Figures 3 and 4. Lines represent the theoretical tendencies based on Eq. (3).

Figure 8. Experimental (rhombs) and theoretical (continuous lines) Nyquist plots corresponding to EIS spectra of coins a) 550612, b) 550600, c) 550597 and d) 550592 partially immersed into air-saturated mineral water; bias potential –0.60 V.

Figure 9. Equivalent circuits used to model the observed EIS responses of the studied coins for the cases of a) moderate and b) gross corrosion.

Figure 10. Plots of $\log R_{ct}$ vs. $\log|Z_{low}|$ for: a) coins 7464, 8934, 8935, 8959 and b) all studied coins using forced fitting to the equivalent circuit in Figure 7. a) Individual values of three replicate measurements and b) average values from three independent replicate experiments for each coin.

Figure 11. Plots of $\log(R_{corr})$ vs. $\log(R_{ct})$ for EIS spectra of the studied coins using forced fitting to the equivalent circuit in Figure 8b. Average values from three independent replicate experiments for each coin.

Figure 1.

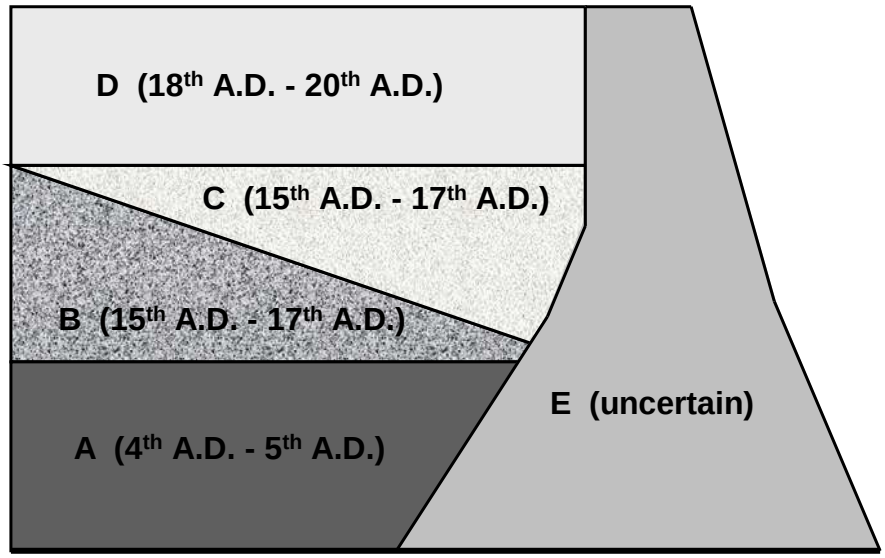
D (18th A.D. - 20th A.D.)
C (15th A.D. - 17th A.D.)
B (15th A.D. - 17th A.D.)
A (4th A.D. - 5th A.D.)
E (uncertain)

Figure 2.

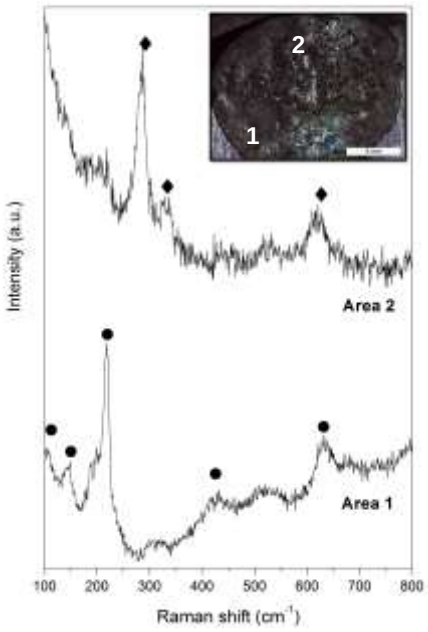
2
1
Area 2
Area 1
Intensity (a.u.)
100
200
300
400
500
600
700
800
Raman shift (cm-1)

Figure 3.

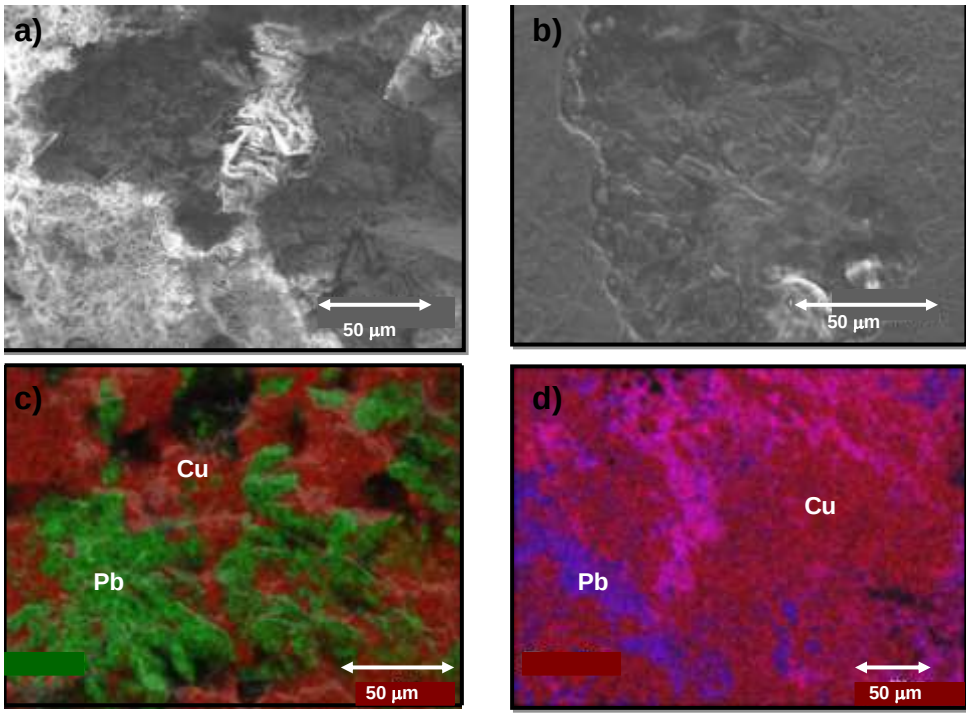

Figure 4.

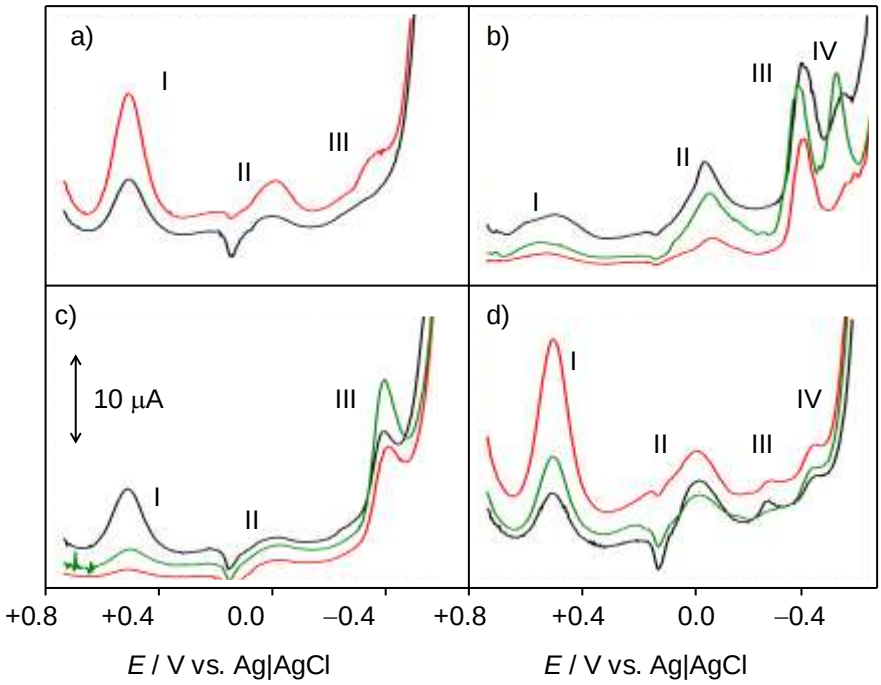
a)
I
II
III
b)
I
II
III
IV
c)
10 μA
I
II
III
d)
I
II
III
IV
+0.8
+0.4
0.0
–0.4
+0.8
+0.4
0.0
–0.4
E / V vs. Ag|AgCl
E / V vs. Ag|AgCl

Figure 5.

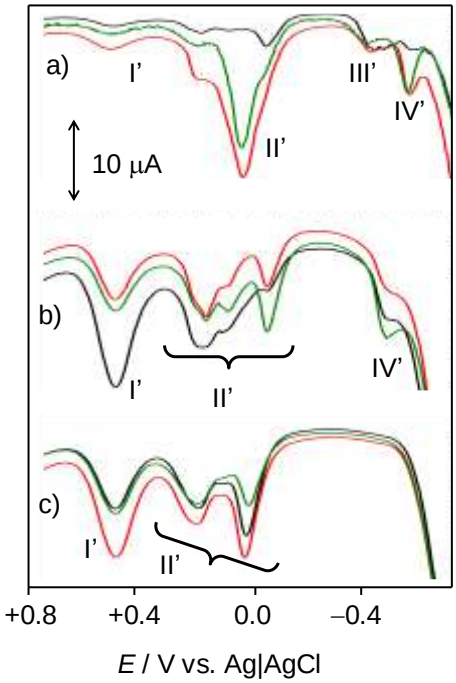

Figure 6.

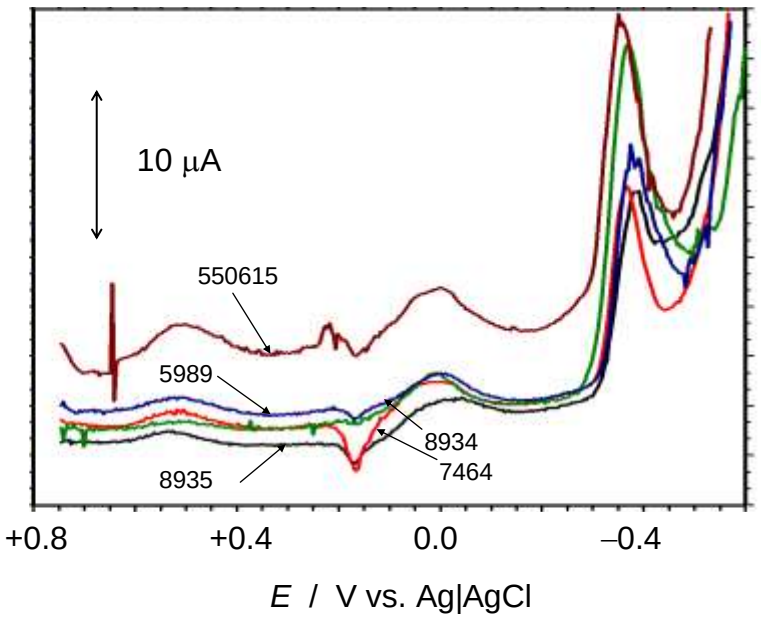

Figure 7.

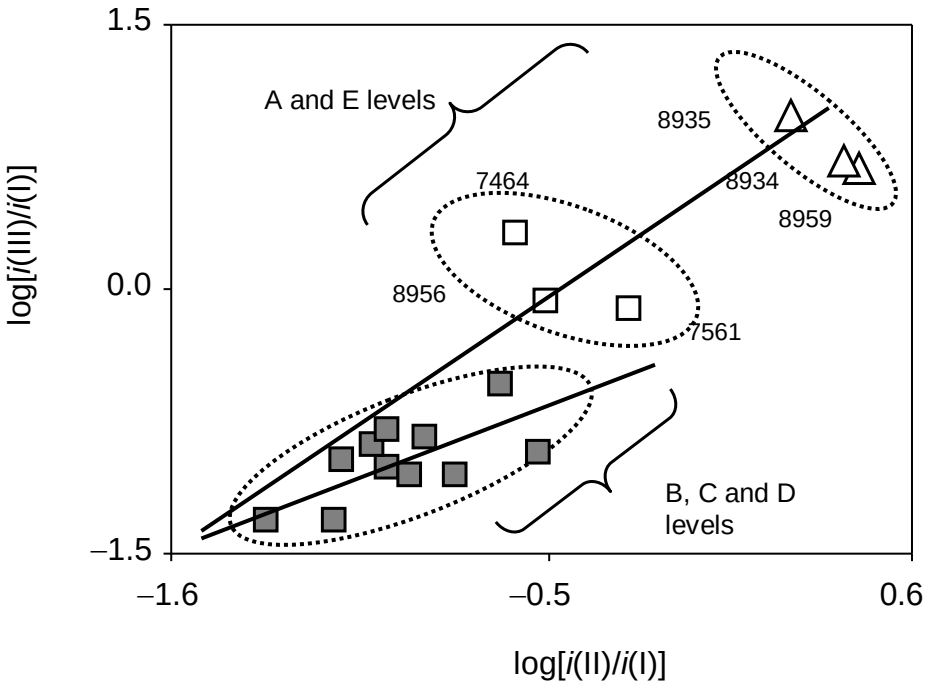
1.5
0.0
–1.5
–1.6
–0.5
0.6
log[*i*(III)/*i*(I)]
log[*i*(II)/*i*(I)]
A and E levels
B, C and D levels
8935
8934
8959
7464
8956
7561

Figure 8.

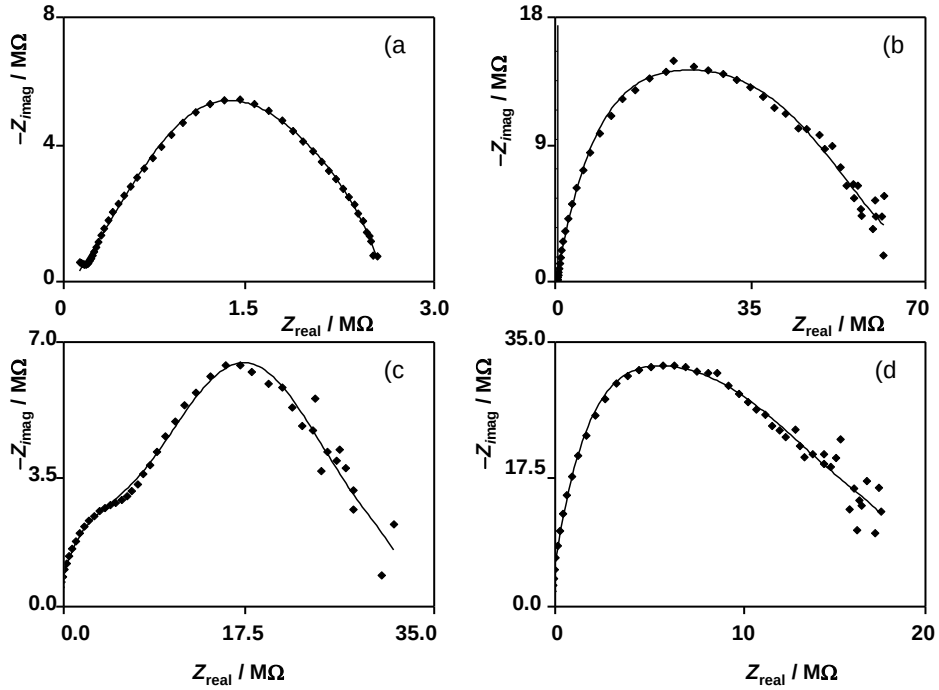

Figure 9.

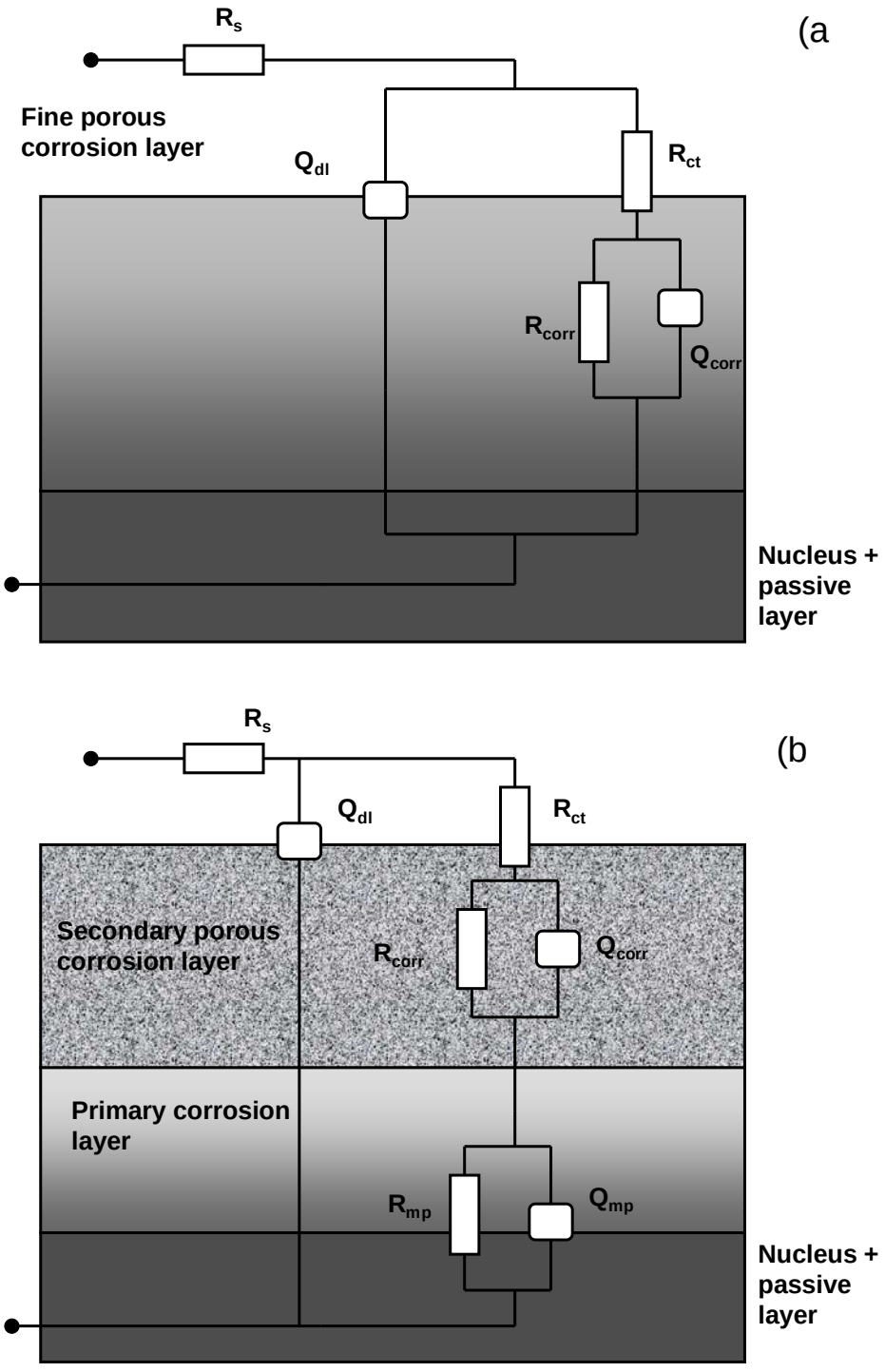
(a
R_s
Fine porous corrosion layer
Q_{dl}
R_{ct}
R_{corr}
Q_{corr}
Nucleus + passive layer
(b
R_s
Q_{dl}
R_{ct}
Secondary porous corrosion layer
R_{corr}
Q_{corr}
Primary corrosion layer
R_{mp}
Q_{mp}
Nucleus + passive layer

Figure 10.

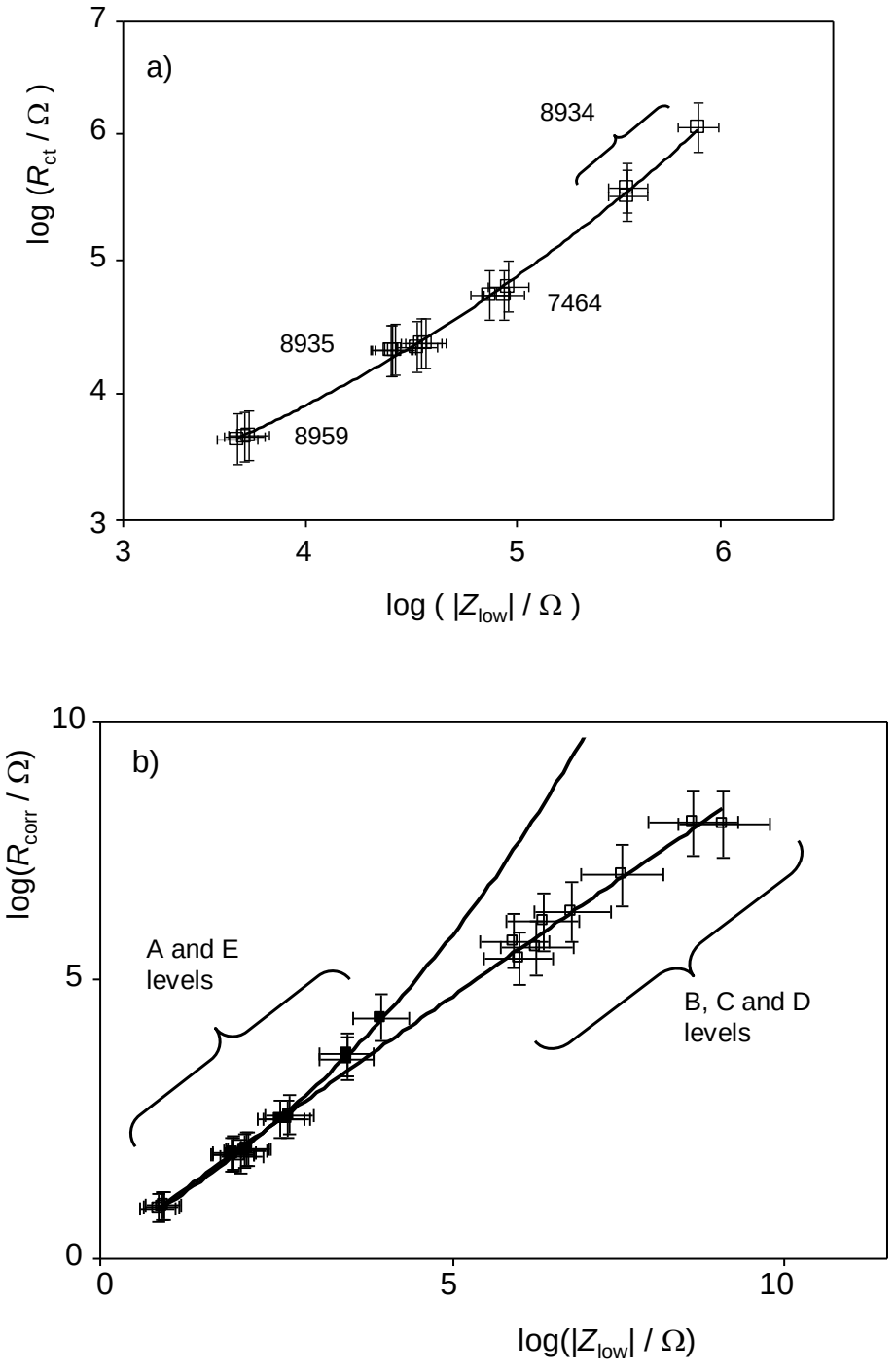
a)
8934
7464
8935
8959
log (R_{ct} / Ω)
log ($|Z_{low}|$ / Ω)
b)
A and E
levels
B, C and D
levels
log(R_{corr} / Ω)
log($|Z_{low}|$ / Ω)

Figure 11.

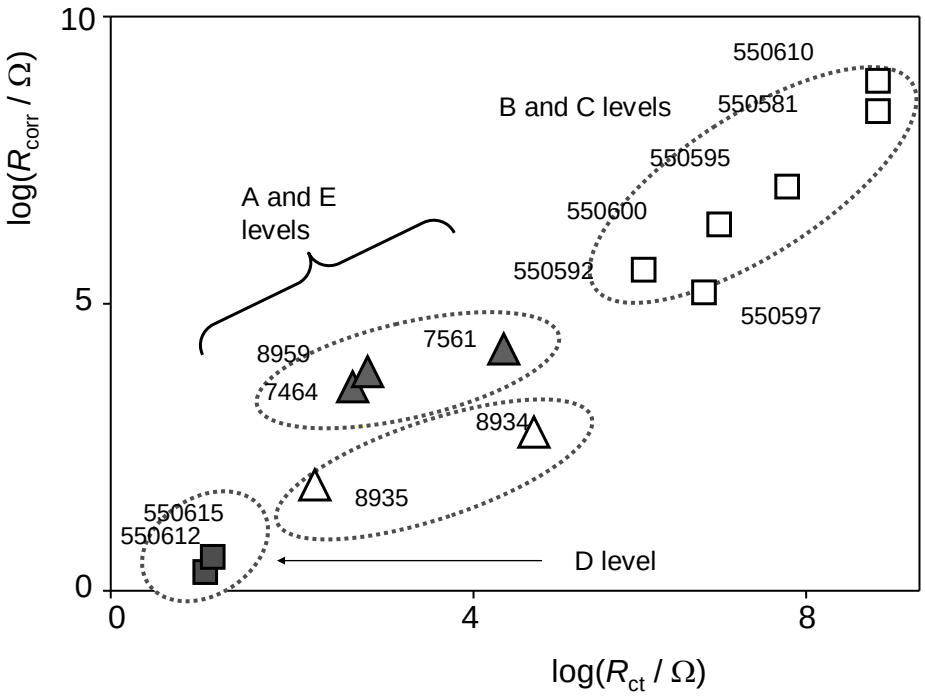
10
5
0
0
4
8
log(R_{corr} / Ω)
log(R_{ct} / Ω)
550610
B and C levels
550581
550595
A and E
levels
550600
550592
550597
8959
7561
7464
8934
8935
550615
550612
D level

Supplementary information

Figure S1. SWVs of a) tenorite, b) cuprite, and samples from the brownish region of coins c) 8959 and d) 550615 attached to graphite electrodes immersed into 0.25 M HAc/NaAc aqueous solution at pH 4.75. Potential scan initiated at +0.75 V in the negative direction; potential step increment 4 mV; square wave amplitude 25 mV; frequency 5 Hz.